Flow Boiling in an Asymmetrically Heated Single Rectangular Microchannel

Cheol Huh[1] and Moo Hwan Kim[2]

[1]Korea Ocean Research and Development Institute (KORDI),
[2]Pohang University of Science and Technology (POSTECH),
Republic of Korea

1. Introduction

Heat transfer and fluid flow in microscale domains are found in many places such as microchannel heat sinks and microfluidic devices. In fact, microfluidic devices are the fastest growing area, and the development of these devices has greatly exceeded our ability to analyze them in detail. A two-phase microchannel heat sink is one of the best candidates for resolving this form of thermal management. Furthermore, limited pumping power capabilities in microscale devices have introduced concerns about large pressure drops in microchannel geometries. Many experimental investigations have been carried out to evaluate the pressure drop and heat transfer for in mini/microchannels. However, heat transfer and fluid flow in the microscale domain frequently display counterintuitive behavior due to the different forces dominating at micro-length scales. Therefore, experimental diagnostic techniques are essential for understanding two-phase pressure drop and flow boiling heat transfer in a microchannel. In addition, to elucidate the boiling heat transfer characteristics without interference from the flow distributor and the interactions between adjacent channels, it is necessary to study two-phase flow in a single microchannel.

A modified Chisholm's C parameter as a function of the hydraulic diameter based on measured the void fraction and frictional pressure drop for air-water flows in capillary tubes with inner diameters in the range of 1 to 4 mm was proposed (Mishima et al., 1993; Mishima & Hibiki, 1996). Two-phase flow pressure drop measurements for three refrigerants: R-134a, R-12, and R-113 were carried out (Tran et al., 2000). The experiments were performed in two round tubes (inner diameters of 2.46 and 2.92 mm) and one rectangular channel (4.06 x 1.7 mm). The measured two-phase frictional pressure drops were not accurately predicted by conventional macro-channel correlations. A new two-phase frictional multiplier based on Chisholm's B-coefficient method (Chisholm, 1973) as a function of the dimensionless physical property coefficient and the confinement number was suggested. Another modified C parameter based on the Lockhart-Martinelli two-phase multiplier was proposed with an air-water two-phase pressure drop experiments in a narrow channel 20 mm in width and 0.4 to 4 mm in height (Lee & Lee, 2001). They proposed a modified C parameter based on the Lockhart-Martinelli two-phase multiplier to take into

account the effects of the viscous and surface tension forces. For small channels, the occurrence of slug flow over a large quality range reduced the pressure gradients from those of the annular flow conditions found in larger tubes (Yu et al., 2002). Recently, a modified Mishima and Hibiki correlation by appending the mass flux effect to the Chisholm's *C* parameter was proposed based on experimental results with 21 parallel channels, 0.231 mm in width and 0.712 mm in height (Qu & Mudawar, 2003).

The local heat transfer coefficient for saturated boiling of R-113 in a 3.1-mm inner diameter round tube was measured (Lazarek & Black, 1982). A simple correlation for the local heat transfer coefficient was presented in the form of a two-phase Nusselt number as a function of the liquid-only Reynolds number and boiling number. Experiments were performed with R-12 in 2.4-mm hydraulic diameter rectangular channels and 2.46-mm circular channels and the boiling heat transfer coefficients were measured (Tran et al., 1996). Those results indicated that the heat transfer coefficients were dependent on the heat flux alone to the higher vapor qualities. The mass flux and vapor quality did not influence the heat transfer coefficients. Other experimental results (Yu et al., 2002) showed a similar trend and the boiling heat transfer correlation to these results. The flow boiling experiments of R-141b in 500-mm-long channels from 1.39 to 3.69 mm in diameter were carried out (Kew & Cornwell, 1997). It was showed that Cooper's nucleate pool boiling correlations predicted the experimental data well. Three flow regimes were observed: isolated bubble flow, which is similar to bubbly flow in a large channel; confined bubble flow, which involves an elongated bubble; and annular-slug flow. The heat transfer coefficient for the evaporation of R134a flowing in a small circular copper tube with an inner diameter of 2 mm was measured (Yan & Lin, 1998). It was showed that the evaporation heat transfer coefficient averaged over the entire vapor quality range was about 30-80% higher than that for a large pipe with an inner diameter of 8.0 mm. The effect of liquid film thickness on heat transfer using a film flow model was conducted based on the flow boiling experiments with R-113 in narrow channels 20 mm wide and 0.4-2 mm height (Lee & Lee, 2001). The major heat transfer mechanism was convective heat transfer and that vapor quality had a stronger effect on the boiling heat transfer as the height of the channel decreased. A thin liquid film evaporation model of an elongated bubble in a microchannel assuming that incepted bubbles grow to the channel size quickly to form successive elongated bubbles was proposed (Jacobi & Thome, 2002). The channel confined the elongated bubbles, forming a thin film of liquid between the bubble and the channel wall. They presented a simple heat transfer model based on the hypothesis that the evaporation of a thin liquid film into elongated bubbles is the important heat transfer mechanism in microchannel evaporation. The flow boiling experiment with FC-84 in five parallel rectangular channels with a hydraulic diameter 0.75 mm was carried out (Warrier et al., 2002). The heat flux was applied using heating strips placed on the top and bottom surfaces of the test channel. A correlation for the saturated flow boiling heat transfer coefficient as a function of boiling number was proposed. Other experimental researches showed that the saturated flow boiling heat transfer coefficients were strongly dependent on the mass flux, and weakly dependent on the heat flux (Qu & Mudawar, 2003). It was reported that annular flow was the dominant two-phase flow pattern in microchannels at moderate and high heat fluxes. Tables 1 and 2 summarize the previous studies and the development of correlations for two-phase frictional pressure drop and flow boiling heat transfer in mini/microchannels.

The objective of this chapter is to gain a fundamental understanding of two-phase pressure drop and flow boiling heat transfer of water in a microchannel. An experimental study of flow boiling heat transfer in a single horizontal microchannel having a hydraulic diameter similar with bubble departure diameter was performed. To elucidate characteristics of the two-phase flow and flow boiling, identify the flow pattern, evaluate the prediction capability of the existing correlations for two-phase frictional pressure gradient and boiling heat transfer coefficient, and develop better predictable correlations, thorough experimental investigations of flow boiling for the quality range of 0-0.4 were conducted. Finally, the elongated bubble behavior in a microchannel was analyzed by comparing experimental observations and numerical calculations.

Author (year)	Fluid	Test conditions	Channel geometry (mm)	Remarks
Mishima and Hibiki (1996)	Air/water	Superficial velocity 0.2-80 m/s (gas) 0.1-1.6 m/s (liquid)	Circular: 1-4; Vertical	Modified Chisholm C parameter
Mishima et al. (1993)	Air/water	Superficial velocity 0.1-10 m/s (gas) 0.2-5 m/s (liquid)	Rectangular gap: 1.0, 2.4, 5.0; Vertical	Modified Chisholm C parameter
Tran et al. (2000)	R-134a, R-12, R-113	P = 138-856 kPa G = 33-832 kg/m²s q'' = 2.2-129 kW/m² x = 0.02-0.95	Circular: 2.46, 2.92; Rectangular: 4.06x1.7; Horizontal	Modified two-phase multiplier based on the Chisholm B coefficient
Lee and Lee (2001)	Air/water	Superficial velocity 0.05-18.7 m/s (gas) 0.03-2.39 m/s (liquid)	Rectangular: 20x0.4-2; Horizontal	Modified Chisholm C parameter
Yu et al. (2002)	Water	P = 200 kPa G = 50-200 kg/m²s q'' = 10-300 kW/m² x = 0.5-0.95	Circular: 2.98; Horizontal	Modified two-phase multiplier for laminar liquid and turbulent vapor
Qu and Mudawar (2003)	Water	P = 1.17 bar G = 135-400 kg/m²s q'' = 400-1300 kW/m² x = 0.5-0.95	Rectangular: 0.231x0.713; Horizontal	Modified Mishima and Hibiki correlation

Table 1. Summary of previous studies on two-phase pressure drop in mini/microchannels (Mishima & Hibiki, 1996; Mishima et al., 1993; Tran et al., 2000; Lee & Lee, 2001; Yu et al., 2002; Qu & Mudawar, 2003)

Author (year)	Fluid	Test conditions	Channel geometry (mm)	Remarks
Lazarek and Black (1982)	R-113	P=0.13-0.41 MPa G=125-750 kg/m²s q"=14-380 kW/m² x=0-0.6	Circular, 3.1, Vertical	Nucleate boiling heat transfer dominant
Tran et al. (1996)	R-12	P=0.51-0.82 MPa G=44-832 kg/m²s q"=3.6-129 kW/m² x=0-0.94	Circular, 2.46 Rectangular, 2.4 Horizontal	Nucleate boiling heat transfer dominant
Kew and Cornwell (1997)	R-141b	G=188-1480 kg/m²s q"=9.7-90 kW/m² x=0-0.9	Circular, 1.39-3.69, Horizontal	Nucleate boiling heat transfer dominant
Yan and Lin (1998)	R-134a	T_{sat}=15, 31 ºC G=50-200 kg/m²s q"=5-20 kW/m² x=0.1-0.9	Circular, 2 28 pipes, Vertical	-
Lee and Lee (2001)	R-113	G=51.6-209 kg/m²s q"=0-16 kW/m² x=0.2-0.8	Rectangular, 20x0.4-2 Horizontal	Convective boiling heat transfer dominant
Warrier et al. (2002)	FC-84	G=557-1600 kg/m²s q"=0-40 kW/m² x=0-0.6	Rectangular, 0.75 parallel Horizontal	-
Yu et al. (2002)	Water	P=200 kPa G=50-200 kg/m²s q"= 0-300 kW/m² x=0.15-1.0	Circular, 2.98, Horizontal	Nucleate boiling heat transfer dominant
Qu and Mudawar (2003)	Water	P=1.17 bar G=135-402 kg/m²s q"=0-1000 kW/m² x=0-0.2	Rectangular, 0.231x0.713 Horizontal	Convective boiling heat transfer dominant

Table 2. Summary of previous studies on flow boiling heat transfer in mini/microchannels (Lazarek & Black, 1982; Tran et al., 1996; Kew & Cornwell, 1997; Yan & Lin, 1998; Lee & Lee, 2001; Warrier et al., 2002; Yu et al., 2002; Qu & Mudawar, 2003)

2. Experimental setup and procedure

2.1 Experimental apparatus

The experimental system consisted of several sub-systems, which included a working fluid loop, test section, flow visualization devices, and data acquisition systems (Huh & Kim, 2006). A schematic diagram of the experimental flow loop configured to supply the test fluid, deionized water, to the test section is shown in Fig.1. Deionized water was delivered to the test section using dual operation syringe pumps through a line filter with a 2 µm screen mesh, which facilitated the removal of solid particles that could contaminate and/or block the flow passage. To adjust the stiffness of the upstream fluid handling system, the test microchannel was located immediately ahead of a metering valve. During the normal

experiments, the metering valve remained fully open. After the test section, the water returned to the outlet reservoir installed on an electronic balance. The mass flow of water was measured by reading the gradient of mass with time from the electronic balance. Two absolute pressure transducers and four type-T thermocouples were installed for the inlet and outlet pressure and temperature measurements. To measure the pressure drop across the test section, a differential pressure transducer was installed between the inlet and outlet of the test section. To allow the real-time flow visualization of flow boiling behaviour in a microchannel, a high-speed CCD camera with a microscope was installed above the test section. Details of the experimental rig were described in the previous work of the present authors (Huh & Kim, 2006).

The test section consisted of a series of microheaters and a single horizontal rectangular microchannel, as shown in Fig. 2. A total of six piecewise serpentine platinum microheaters, separated from each other, was fabricated along the flow direction by using a surface micromachining Micro-Electro-Mechanical Systems (MEMS) technique. In single microchannel flow boiling experiments, it is difficult to add an external pre-heater that controls the test section inlet fluid temperature because the heat and fluid flow are too small to maintain the thermodynamic state of the inlet fluid without heat losses. The six microheaters were controlled separately and monitored to determine the roles of the pre-heater and main heater. To evaluate the heat input from the microheaters to the working fluid, the voltage and current in each microheater was measured using an Agilent 34901A module. It is believed that most of the heat generated by the platinum is concentrated in the area of the central serpentine pattern corresponding to the microheater due to the very large line width ratio of the lead line pattern to the serpentine pattern. Since a linear relationship exists between resistance and temperature in platinum, platinum microheaters perform as both heaters and temperature sensors at the heated surface along the flow direction. To quantify the relationship between temperature and the resistance of each microheater, each microheater was calibrated in a constant-temperature convection oven after allowing sufficient time to achieve thermodynamic equilibrium. Each microheater showed a fairly good linear relationship between temperature and resistance.
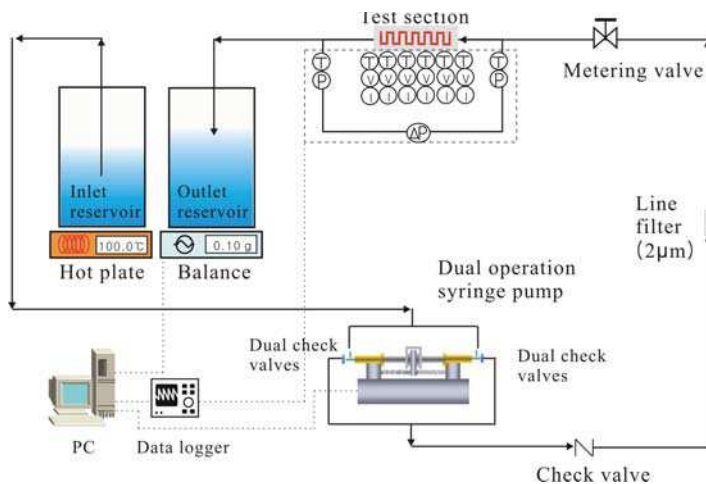

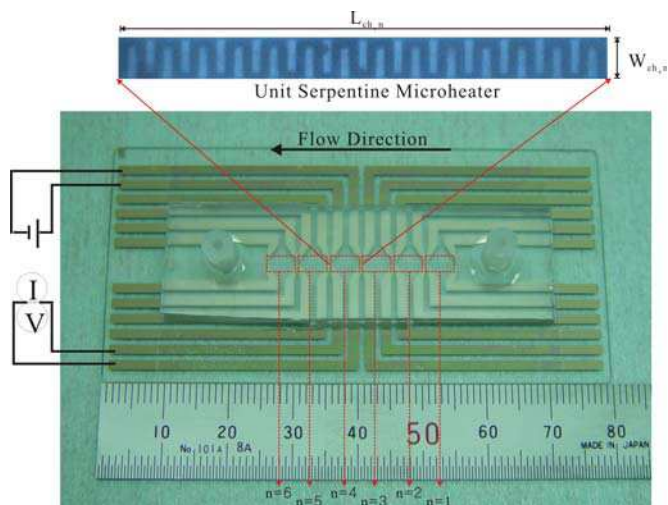Fig. 1. Schematic diagram of the test apparatus

Fig. 2. Test section (microheaters and microchannel)

A horizontal rectangular microchannel with a hydraulic diameter of 100 μm and an aspect ratio of 1.0 was manufactured using a replica molding technique. Polydimethylsiloxane (PDMS) was selected as the structural material of the microchannel because of its low thermal conductivity and transparency to visible light. Therefore, it could serve as insulation without obstructing observations of the flow patterns. Although PDMS has good insulating and optical properties, preliminary test results showed the strong influence of the permeability and porosity of the bare PDMS. In order to prevent premature bubbles from forming in the microheaters and microchannel, both the inner and outer walls of the microchannel were coated with Parylene C Dimer (di-chloro-di-para-xylyene). Parylene film has low permeability to moisture and gases. Details of the microheaters and the microchannel fabrication procedures in the present study were described in the previous work of the present authors (Huh & Kim, 2006).

2.2 Test conditions and procedures

After the flow became stable, as determined by monitoring mass flux, inlet pressure, and differential pressure across the test section, the heater powers were increased in small increments with digital precision DC power supplies (Huh & Kim, 2006). Then the test loop components were constantly adjusted to maintain the desired operating conditions. The experimental conditions are mass fluxes of 90-363 kg/m²s, volume flow rates of 0.05-0.2 ml/min, all liquid Reynolds number of 9-40, and heat fluxes of 200-700 kW/m². Simultaneously, the mass flow of water was measured by reading the gradient of mass with time from the electronic balance through a RS-232 interface. The test data were collected using a data acquisition system consisting of data loggers, an interface device (GPIB to USB), and a personal computer. The two-phase frictional pressure gradient and flow boiling heat transfer coefficient was obtained from the average value of the calculated data with an in-house data reduction program. The thermodynamic and transport properties of water were calculated based on the NIST standard reference database found in the NIST chemistry webbook (http://webbook.nist.gov/).

2.3 Data reduction

The microchannel had six microheaters on the bottom wall of the channel along the flow direction. Subcooled water was supplied from the inlet reservoir to the test microchannel. Therefore, the microchannel could be divided into single-phase liquid regions and two-phase mixture regions, as shown in Fig. 3. Details of the data reduction method in the present study were described in the previous work of the present authors (Huh & Kim, 2006; Huh et al., 2007). The dividing point between the single-phase and two-phase region was determined from the thermodynamic equilibrium quality based on an energy balance evaluation at each region. It was assumed that the exact position of zero thermodynamic equilibrium quality existed at the midpoint between the last section of the single-phase region and the first section of the two-phase region.
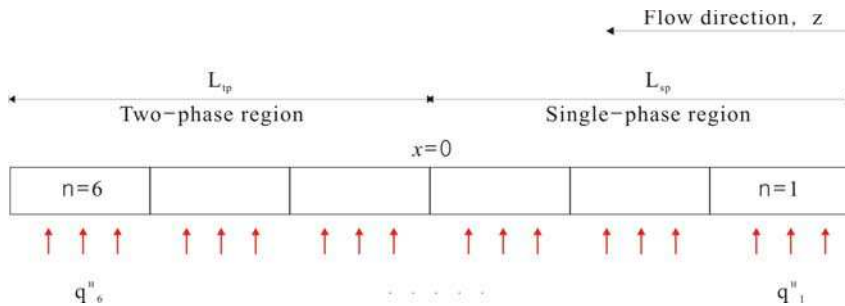
Fig. 3. The six microheater and microchannel sections

The heat generated by Joule heating and lost to the environment was taken into account to determine the effective heat input from the microheaters to the test fluid as follows. As described elsewhere (Huh and Kim, 2006), the total heat generation, q_n, and heat loss, $q_{loss,n}$, the effective heat flux $q''_{eff,n}$ and the exit qualities at the n-th microheater/microchannel section were calculated as follows:

$$q_n = V_n\, I_n \tag{1}$$

$$q_{loss,n} = \frac{k_{bw,n}\left(T_{h,n} - T_{bw,n}\right)}{H_{bw,n}} W_{ch,n} L_{ch,n} \tag{2}$$

$$q''_{eff,n} = \frac{q_n - q_{loss,n}}{W_{ch,n} L_{ch,n}} \tag{3}$$

$$x_{out,n} = \frac{\sum_n q_{eff,n} - \sum_{sub,n} q_{eff,n}}{\dot{m}_f i_{fg}} \tag{4}$$

where V_n is the electric voltage, I_n is the electric current, $k_{bw,n}$ is the thermal conductivity of the bottom wall, $H_{bw,n}$ is the thickness of the bottom wall, $T_{h,n}$ is the temperature of the heated surface, $T_{bw,n}$ is the temperature of the bottom wall, and $W_{ch,n}$ and $L_{ch,n}$ are the width and length of the microchannel, respectively. The required sensible heat, $\Sigma_{sub,n}\, q_{eff,n}$, was subtracted from the total effective heat input, $\Sigma_n\, q_{eff,n}$, between the inlet of the test section to the section n. And $\dot{m}_f$ is the mass flow rate of the test fluid and i_{fg} is the latent heat of

vaporization. Since the pressure drop between the inlet and outlet of the test section was measured using a differential pressure transducer installed across the test section, the measured pressure drop was the sum of the pressure drops across the test section. The total measured pressure drop could be divided into five components: the test section inlet pressure drop (Δp_{inlet}), the single-phase frictional pressure drop ($\Delta p_{f,sp}$), the two-phase frictional pressure drop ($\Delta p_{f,tp}$), the acceleration pressure change (Δp_{acc}), and the test section outlet pressure change (Δp_{outlet}):

$$\Delta p_{\exp} = \Delta p_{inlet} + \Delta p_{f,sp} + \Delta p_{f,tp} + \Delta p_{acc} + \Delta p_{outlet} \tag{5}$$

The inlet pressure change due to the sudden contraction at the inlet was estimated as

$$\Delta p_{inlet} = p_{in} - p_{out} = \frac{G_{out}^2 \upsilon_f}{2} \left[1 - \left(\frac{A_{cross,out}}{A_{cross,in}} \right)^2 + K_{inlet} \right] \tag{6}$$

where G is the mass flux, υ_f is the specific volume of liquid, and A is the cross-sectional area of the channel. The irreversible contraction loss coefficient, K_{inlet}, can be obtained from the literature (Blevins, 1984) and the subscripts *in* and *out* refer to the corresponding fluid connection. The single-phase region can be further divided into developing and fully developed regions. For the present study, the Reynolds number of the test range was within the laminar flow range and the length of the single-phase developing region can be neglected due to its small value. The single-phase frictional pressure drop was calculated as

$$\Delta p_{f,sp} = \frac{f}{2} G_{out}^2 \upsilon_f \frac{L_{sp}}{D_h} \tag{7}$$

where f is the dimensionless friction factor, L_{sp} is the length of the single-phase region including the adiabatic length before the heated region, and D_h is the hydraulic diameter of the channel. The dimensionless friction factor, fRe=15.25, for single-phase liquid flow was obtained from single-phase adiabatic experiments of the present study. The pressure increment caused by the sudden enlargement at the outlet can be calculated (Collier & Thome, 1994):

$$-\Delta p_{outlet} = p_{out} - p_{in} = G_{in}^2 \left(\frac{A_{cross,in}}{A_{cross,out}} \right) \left[1 - \left(\frac{A_{cross,in}}{A_{cross,out}} \right) \right] \upsilon_f \left[\frac{(1-x)^2}{(1-\alpha)} + \left(\frac{\upsilon_g}{\upsilon_f} \right) \frac{x^2}{\alpha} \right] \tag{8}$$

where x is the quality of the two-phase mixture, υ is the specific volume, α is the void fraction of the two-phase mixture, and subscripts f and g indicate liquid and vapour, respectively. The pressure change caused by acceleration due to the phase change along the test channel can be estimated as

$$\Delta p_{acc} = p_{out} - p_{in} = -G^2 (\upsilon_{out} - \upsilon_{in}) = -G^2 \upsilon_{fg} \Delta x \tag{9}$$

Finally, the two-phase frictional pressure drop, $\Delta p_{f,tp}$, can be obtained from the measured overall pressure drop using Eqs. (5)-(9).

The flow boiling heat transfer coefficient at the n-th section was calculated using

$$h_{TP,n} = \frac{q''_{eff,n}}{T_{h,n} - T_{sat,n}} \tag{10}$$

where the saturation temperature of the water at the n-th section, $T_{sat,n}$, was calculated with the local pressure of the water at that section, considering single- and two-phase pressure drops. To determine the local saturation temperature, the local saturation pressure in the two-phase region is assumed to be linearly distributed along the channel.

2.4 Experimental uncertainties

The data reduction equation for the flow boiling heat transfer coefficient was derived from Eq. (10) and the experimental uncertainties (Holman , 2001) are represented as follows:

$$\frac{u_{h_{TP,n}}}{h_{TP,n}} = \sqrt{\left(\frac{u_{q''_{eff,n}}}{q''_{eff,n}}\right)^2 + \left(\frac{u_{T_{h,n}}}{T_{h,n} - T_{sat,n}}\right)^2 + \left(\frac{u_{T_{sat,n}}}{T_{h,n} - T_{sat,n}}\right)^2} \tag{11}$$

where, $u_{h_{TP,n}}$, $u_{q''_{eff,n}}$, $u_{T_{h,n}}$, and $u_{T_{sat,n}}$ are the uncertainties of the heat transfer coefficients, effective heat flux, heated surface temperature, and saturation temperature of the test fluid at the n-th section, respectively. The estimated experimental uncertainties obtained from this analysis are shown in Table 3.

Parameter	Uncertainty
Temperature	± 0.1 °C
Pressure	± 0.76 kPa
Pressure difference	± 0.34 kPa
Volume flow rate	± 0.1%
Mass Flux	± 1.09%
Heat Flux	± 2.74%
Vapor Quality	0.025
Heat Transfer Coefficient	±3.3 ~ ±10.1%

Table 3. Experimental uncertainties

The experimental uncertainty of the outlet quality in the two-phase sections is about half of the difference in the quality between adjacent two-phase regions. Accounting for all of the instrument errors, the estimated uncertainties for the average heat transfer coefficient ranged from ±3.3 to ±10.1%.

3. Results and discussion

3.1 Single-phase pressure drop

Prior to performing the two-phase experiments, the friction factor for the single-phase liquid flow was evaluated. Based on the single phase flow experimental data, a new modified friction factor fRe = 15.25 was obtained. This was used to evaluate the two-phase frictional pressure drop, as described in the previous section. The application range of this modified

new friction factor is limited to a rectangular channel with an aspect ratio of 1.0 due to its originality.

3.2 Two-phase frictional pressure drop

The two-phase pressure drop consists of frictional, accelerational and gravitational pressure drops. The accelerational pressure drop was estimated with Eq. (9) and the gravitational pressure drop was considered to be negligible due to the very small flow passage. A two-phase frictional pressure gradient was determined by dividing the two-phase frictional pressure drop, $\Delta p_{f,tp}$, by the test channel length occupied by liquid and vapor mixture, L_{tp}. Figure 4 shows the effect of the heat and mass fluxes on the two-phase frictional pressure gradient. The two-phase frictional pressure gradient increased with the heat flux, while for a given heat flux, the two-phase frictional pressure gradient increased as the mass flux decreased.
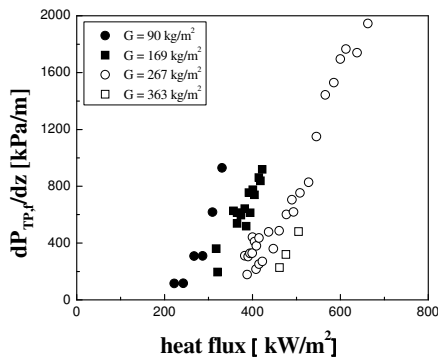
(a) effect of the heat and mass fluxes
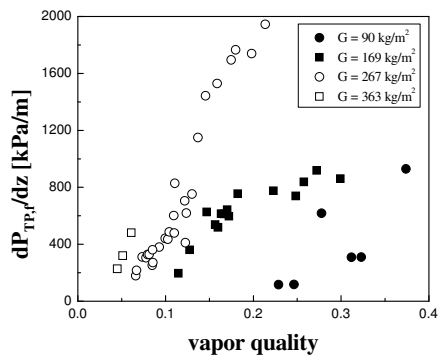
(b) effect of the vapor quality

Fig. 4. The effect of heat flux, mass flux, and vapor quality on two-phase frictional pressure gradient

This indicates that the two-phase pressure drop increased with the vapor quality. As the vapor quality increased, the contribution of the single-phase frictional pressure drop decreased while that of the two-phase frictional pressure drop increased.
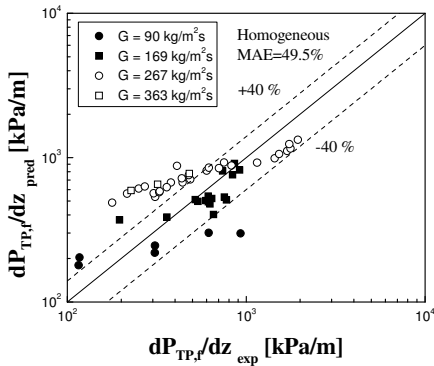
(a) homogeneous flow model
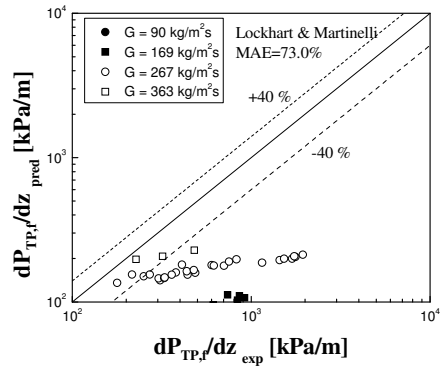
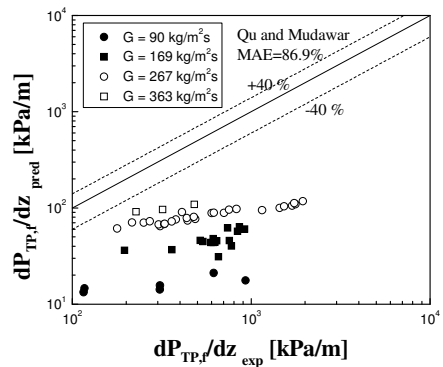(b) Lockhart & Martinelli correlation
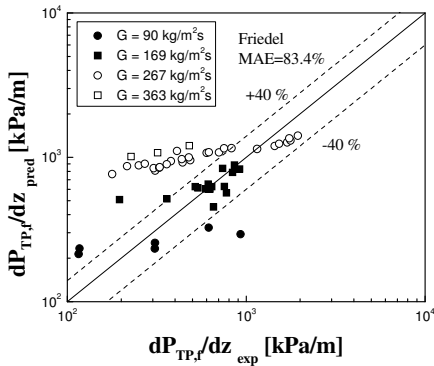
(c) Friedel correlation
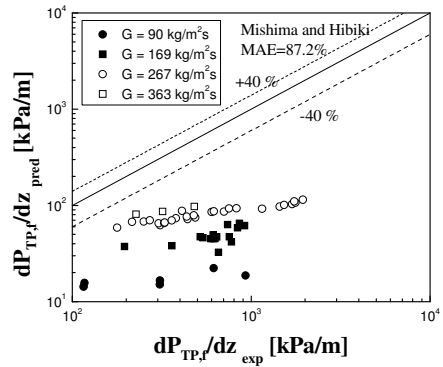
(d) Mishima & Hibiki correlation
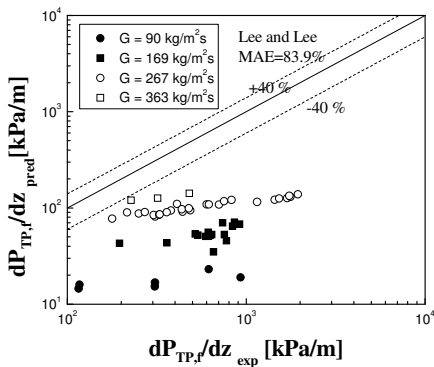
(e) Lee & Lee correlation

(f) Qu & Mudawar correlation

Fig. 5. Comparison of the two-phase frictional pressure gradient with predictions

3.2.1 Two-phase frictional pressure gradient predictions

A large number of correlations previously developed under the framework of the homogeneous equilibrium flow model or the separated flow model were used to evaluate the frictional two-phase pressure drop measured in this study. A total of six empirical correlations, including three macro-channel correlations (Lockhart & Martinelli, 1949, as cited in Collier & Thome, 1994; Friedel, 1979, as cited in Whalley, 1987) including the homogeneous flow model (Collier & Thome, 1994) and three mini/microchannel correlations (Mishima & Hibiki, 1996; Lee & Lee, 2001; Qu & Mudawar, 2003) were examined. Comparisons of the above correlations with the experimental two-phase frictional pressure gradient data are shown in Fig. 5. The homogenous flow model and the Friedel correlation predicted the experimental data well at low flow rate conditions, but did not perform well at high flow rate conditions. On the other hand, the Lockhart and Martinelli and all the mini/microchannels correlations under-predicted the two-phase frictional pressure gradient by large margins at all flow rate conditions. The mean absolute error (MAE, Qu & Mudawar, 2003) was used to provide the relative accuracy of each set of predictions:

$$MAE = \frac{1}{M} \sum \frac{\left| \dfrac{dP_{TP,f}}{dz}_{pred} - \dfrac{dP_{TP,f}}{dz}_{exp} \right|}{\dfrac{dP_{TP,f}}{dz}_{exp}} \times 100\% \tag{12}$$

where $dP_{TP,f}/dz$ is the two-phase frictional pressure gradient, M is the number of data points, and the subscripts *pred* and *exp* indicated the predicted and experimental values, respectively.

The discrepancies between the predictions from the existing correlations and the experimental data were caused by several factors. First, the macro-channel correlations were based on channels that were much larger than microchannel. Second, the most of the existing macro-channel and mini/microchannel correlations were based on turbulent liquid/turbulent vapor or laminar liquid/turbulent vapor flow conditions. However, the flow in microchannel tested in this study was mostly laminar liquid/laminar vapor flow because of the small channel size and low flow rates. Therefore, it is highly desirable to develop a new correlation.

3.2.2 Development of a modified two-phase frictional pressure gradient correlation

The two-phase frictional pressure gradient was analyzed using the two-phase multiplier as follows:

$$\phi_f^2 = \left(\frac{dP}{dz} \right)_{TP} \bigg/ \left(\frac{dP}{dz} \right)_f \tag{13}$$

where $(dP/dz)_{TP}$ is the measured two-phase pressure gradient and $(dP/dz)_{TP}$ is the frictional pressure gradients that correspond to the cases of the liquid flowing alone in the test channel. Based on the experimental results, the two-phase multiplier decreased with the Martinelli parameter, as shown in Fig. 6. These two parameters were used to produce a simple new correlation. The Lockhart-Martinelli correlation with the Chisholm *C* parameter is

$$\phi_f^2 = 1 + \frac{C}{X} + \frac{1}{X^2} \tag{14}$$

$$X^2 = \left(\frac{dP}{dz}\right)_f \bigg/ \left(\frac{dP}{dz}\right)_g \tag{15}$$

where C is a constant that depends on the laminar and turbulent flow regimes of the liquid and vapor and the Martinelli parameter, X^2, is the ratio of the pressure drop caused by the liquid and vapor. As shown in Fig. 6, the two-phase multiplier increased with the vapor quality and decreased with the Martinelli parameter. The Lockhart-Martinelli correlation under-predicted the experimental data, as shown in Figs. 7. In this study, the two-phase multiplier was simply correlated as a power function of the Martinelli parameter, as shown in Fig. 7:

$$\phi_f^2 \propto \frac{1}{X^{3.61}} \tag{16}$$
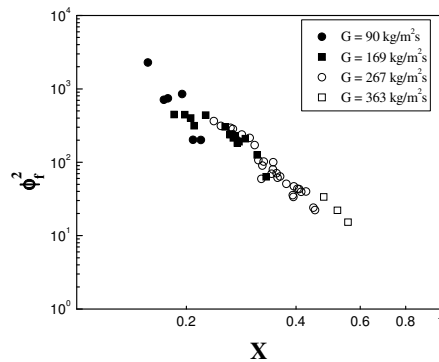
(a) effect of the Martinelli parameter
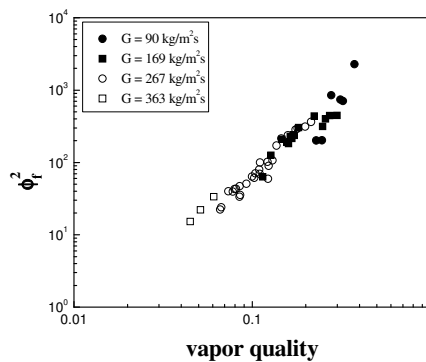
(b) effect of the vapor quality

Fig. 6. Two-phase multiplier: the effect of the (a) Martinelli parameter and (b) vapor quality

To reconcile this simple power function with the Lockhart-Martinelli correlation, the following superposition function was developed:

$$\phi_f^2 = 1 + \frac{C}{X} + \frac{1}{X^2} + \frac{1.62}{X^{3.61}} \tag{17}$$

As shown in Fig. 7(a), the proposed modified two-phase multiplier predicted the experimental data well. Fig. 7(b) compares the experimental two-phase frictional pressure gradient and the predictions from the proposed correlation. The MAE of the proposed correlation was 42%, the lowest value in this study.
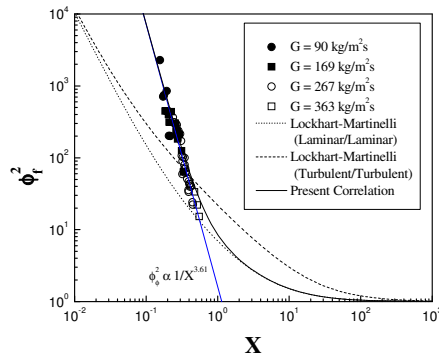
(a) function of the Martinelli parameter
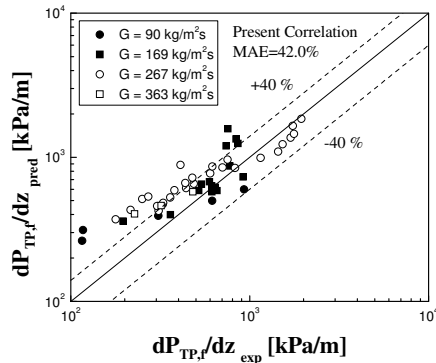
(b) comparison with experimental data

Fig. 7. Development of a new two-phase multiplier correlation as a function of the Martinelli parameter and comparison of the two-phase frictional pressure gradient with the proposed correlation predictions

3.3 Flow boiling heat transfer
3.3.1 Correction for an asymmetric thermal boundary condition
Many empirical correlations for the flow boiling heat transfer coefficient were developed for a circular tube with uniform circumferential heating. However, most of the practical heat transfer on a microscale involves heat transfer along only one or three walls of a rectangular

microchannel. To accommodate these different thermal boundary conditions due the asymmetric heating conditions in our apparatus, a correction method was introduced (Qu & Mudawar, 2003).

$$h_{TP} = h_{TP,correlation} \frac{Nu_1}{Nu_4} \tag{18}$$

where $h_{TP,correlation}$ is the heat transfer coefficient evaluated from a correlation, and Nu_1 and Nu_4 are the single-phase fully developed laminar flow Nusselt numbers for single- and four-wall heat transfer, respectively. The expressions for the single-phase Nusselt number of a rectangular channel with asymmetric heating boundary conditions was used (Shah & London, 1978):

$$Nu_1 = 8.229(1 - 2.197\beta + 4.090\beta^2 - 4.844\beta^3 + 3.437\beta^4 - 1.049\beta^5) \tag{19}$$

$$Nu_4 = 8.235(1 - 2.042\beta + 3.085\beta^2 - 2.477\beta^3 + 1.058\beta^4 - 0.186\beta^5) \tag{20}$$

where $\beta = W_{ch}/H_{ch}$ is the aspect ratio of the rectangular channel. This correction method can be justified due to the fact that the laminar thin liquid film along the microchannel wall contribute the major heat transfer as shown in the flow patterns in the following section.

3.3.2 Flow boiling heat transfer

It is commonly believed that two mechanisms govern heat transfer in saturated flow boiling: nucleate boiling and forced convective boiling (Whalley, 1987; Collier and Thome, 1994; Kandlikar et al., 1999). In the region dominated by nucleate boiling, bubbles are formed by nucleation at the superheated wall. The nucleate boiling heat transfer mechanism is a combination of bubble agitation, thermal boundary layer stripping, and evaporation. The heat transfer coefficient in this region is dependent on the heat flux, and is less sensitive to the mass flux and vapor quality. The nucleate boiling region is normally associated with the bubbly and slug flow patterns. In the region dominated by forced convective boiling, heat is carried away from the heated wall by forced convection in a thin liquid film to the liquid-vapor interface, where evaporation occurs. The heat transfer coefficient in this region is dependent on the mass flux and vapor quality, and is less sensitive to the heat flux. The forced convective boiling region is normally associated with the annular flow pattern.

All heat transfer coefficients and observed flow patterns reported in this paper were measured and evaluated at the last section, $n=6$. The measured flow boiling heat transfer coefficients slightly increased with vapor quality until $x = 0.15$ and were independent of the mass flux and vapor quality for high quality, $0.4 > x > 0.15$, as shown in Fig. 8. The weak dependency of the boiling heat transfer coefficient on the mass flux and vapor quality indicates that the major heat transfer mechanism is nucleate boiling. Although the heat transfer coefficient behaves as if nucleate boiling is the dominant heat transfer mechanism, the major flow pattern is similar to conventional annular flow. The main flow pattern observed at this section is rapid, long elongated slug bubble flow acting like annular flow, as shown in Fig. 9. For the most of the time, the flow pattern looks like thin liquid film flow at the heated wall and vapor flow in the core, as in annular flow. For lower vapor quality region, $x < 0.15$, intermittent vapor zone was appeared during the long elongated slug

bubble flow, as shown in Fig. 10. Figure 10 shows the flow pattern at the mass flux of 267 kg/m²s, the heat flux of 565.9 kW/m², and vapor quality of 0.14. Figures 9 and 10 show the unique flow patterns in the micro-scale flow due to the confined geometry of the microchannel. This flow pattern seldom appears in the conventional large channel at the same vapor quality. For higher vapor quality region, $0.4 > x > 0.15$, the major flow pattern is slug-annular or annular flow, as shown in Fig. 11 captured at the mass flux of 169 kg/m²s, the heat flux of 422.3 kW/m², and vapor quality of 0.27.

Although the observed flow pattern does not support the nucleate boiling mechanism associated with independence of the heat transfer coefficient of the mass flux or vapor quality, the fast and long elongated slug bubbles grown from a single bubble contribute the majority of the heat transfer in the microchannel. This is attributable to the continual supply of heat through a thin liquid film and the continual growth of the elongated bubble. These phenomena result in nucleate boiling-like heat transfer coefficient behavior and convective boiling-like flow patterns. This characteristic of the flow boiling is unique to microchannel, and is not observed in the macro-channels.
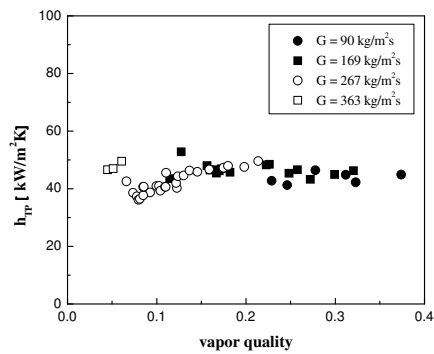
Fig. 8. Effect of the mass flux and vapor quality on the boiling heat transfer coefficients
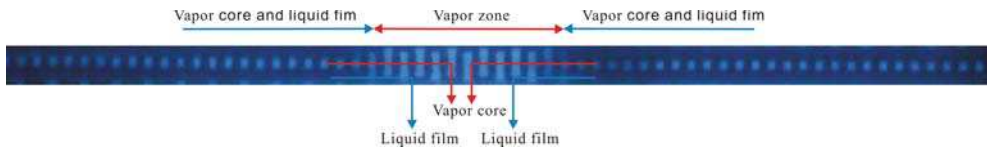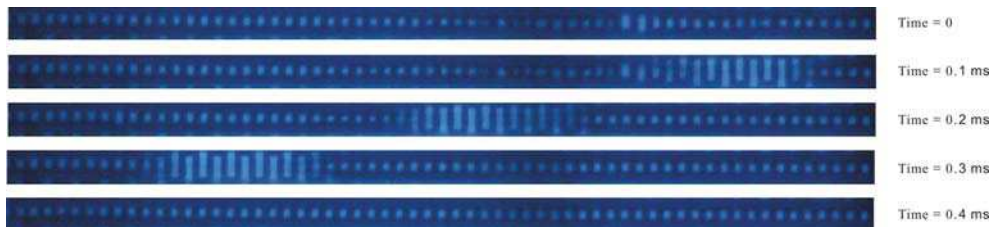

Fig. 9. Elongated slug bubble flow

Fig. 10. Elongated slug bubble flow at G = 267 kg/m²s, q'' = 565.9 kW/m², and x = 0.14

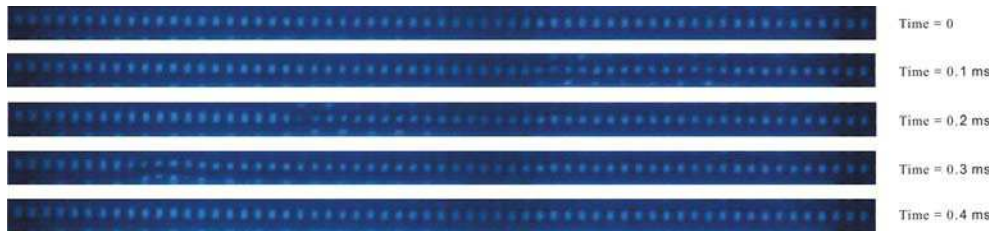Fig. 11. Annular flow at G = 169 kg/m²s, q'' = 422.3 kW/m², and x = 0.27

3.3.3 The predictions of the flow boiling heat transfer coefficient

Six empirical correlations, including three macro-channel correlations (Chen, 1966, as cited in Collier & Thome, 1994; Shah, 1976, as cited in Collier & Thome, 1994; Kandlikar, 1990) and three mini/microchannel correlations (Lazarek & Black, 1982; Yu et al., 2002; Warrier et al., 2002), were examined. As described in the previous section, two kinds of heat transfer mechanisms are superimposed in the flow boiling. For the macro-channel correlations, there are three methods for modelling the heat transfer coefficient: one that adds two components corresponding to the two mechanisms, one that selects the greater of the two components, and one that combines the two components using a power-type asymptotic method. In contrast, the mini/microchannel correlations use a single form combining the two mechanisms.
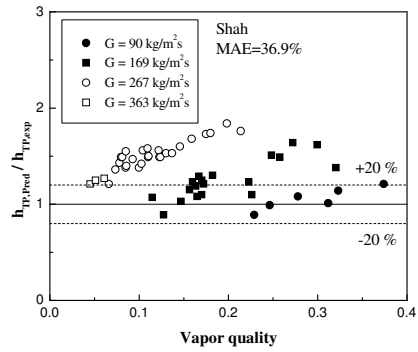
Figure 12 compares the experimental heat transfer coefficients and predictions by the above correlations. Although many of the macro-channel correlations over-predicted the boiling heat transfer coefficient by a large margin, the Chen correlations predicted the experimental data with reasonable accuracy. Most of the macro-channel correlations predicted an increasing heat transfer coefficient with increasing quality, while the experimental data did not show dependency on the vapor quality. The mini/microchannel correlations under-predicted the experimental data over the entire quality range, except the predictions of Lazarek and Black correlation. These comparisons showed that most of the previous correlations are not sufficiently accurate in the microchannel. To quantify the prediction capability of these correlations, we used the mean absolute error (MAE, Qu & Mudawar, 2003). The ratio of the predicted boiling heat transfer coefficients to the experimental data and MAE of each correlation are compared in Fig. 12:

$$MAE = \frac{1}{M}\sum \frac{\left| h_{TP,pred} - h_{TP,\exp} \right|}{h_{TP,\exp}} \times 100\% \tag{21}$$

where h_{TP} is the flow boiling heat transfer coefficient. After assessing the reported boiling heat transfer correlations, it should be emphasized that a difference exists between the correlations and the experimental data. First, the macro-channel correlations are based on a larger test channel than a microchannel, as previously pointed out. Second, most existing macro-channel correlations were developed based on turbulent liquid and turbulent vapor flow conditions. The mini/microchannel correlations are based mainly on laminar liquid and turbulent vapor flow conditions.
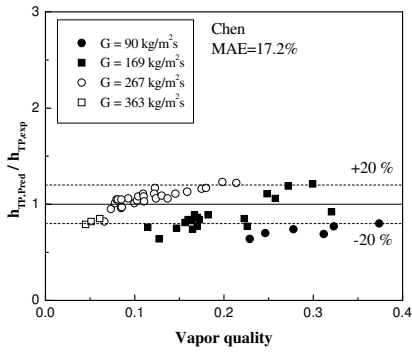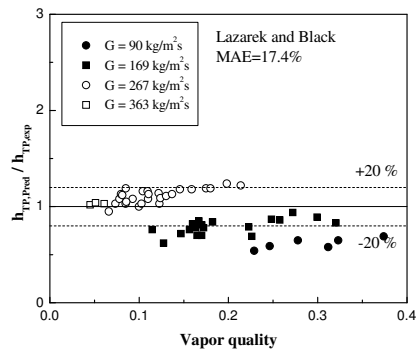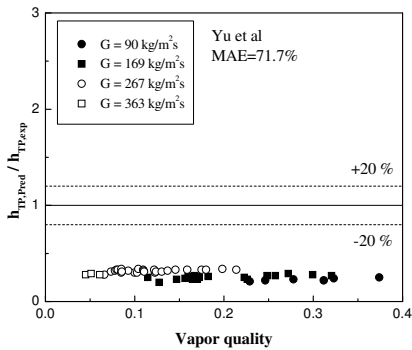
(a) Chen correlation

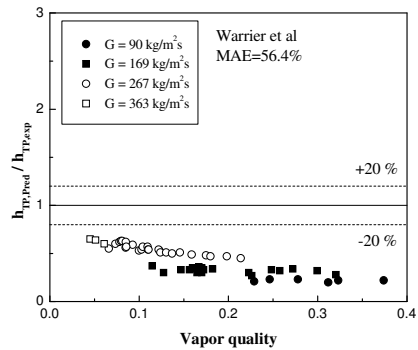(b) Shah correlation
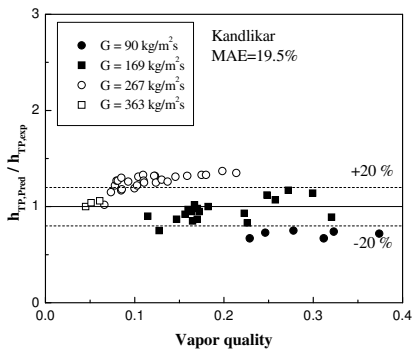
(c) Kandlikar correlation

(d) Lazarek & Black correlation

(e) Yu correlation

(f) Warrier correlation

Fig. 12. Comparison of the experimental boiling heat transfer coefficients and mini/microchannel correlation predictions at section n=6

However, the flow in our microchannel was mostly laminar liquid and laminar vapor flow because of the small channel size and low flow rates. Therefore, a new correlation is highly desired.

3.3.4 Development of a modified flow boiling heat transfer coefficient

The experimental data showed that the boiling heat transfer coefficient does not depend on the mass flux and vapor quality. Although the boiling heat transfer coefficients reflect the nucleate boiling heat transfer mechanism, the major flow patterns are similar to annular flow, as shown in Figs. 8 to 11. In this study, the effect of mass flux can be eliminated by introducing the product of the square of the boiling number and liquid Webber number as follows:

$$Bo^2 We_f = \frac{q''^2}{G^2 i_{fg}^2} \frac{G^2 D}{\rho_f \sigma} = \left(\frac{q''}{i_{fg}} \right)^2 \frac{D}{\rho_f \sigma} \tag{22}$$

where $Bo = q'' / G\, i_{fg}$ is the boiling number and $We_f = G^2 D / \rho_f \sigma$ is the liquid Webber number. Recently, two new non-dimensional groups (Kandlikar, 2001, 2004) are thought to be important in microchannel flow boiling. Of them, the new non-dimensional group K_2 represents the ratio of the evaporation momentum and surface tension forces:

$$K_2 = \frac{\left(\dfrac{q''}{i_{fg}} \right)^2 \dfrac{D}{\rho_g}}{\sigma} = \left(\frac{q''}{i_{fg}} \right)^2 \frac{D}{\rho_g \sigma} \tag{23}$$

The non-dimensional group K_2 governs the movement of the liquid and vapor interface at the contact line. A high evaporation momentum force causes the interface to overcome the retaining surface tension force. Interestingly, the new non-dimensional group K_2 and the liquid and vapor density ratio ρ_g/ρ_f can replace the product of the boiling number and Webber number as follows:

$$Bo^2 We_f = K_2 \frac{\rho_g}{\rho_f} \tag{24}$$

In this study, the boiling heat transfer coefficient can be expressed as the following function:

$$h_{TP} \propto Bo^2 We_f \frac{\rho_g}{\rho_f} \propto K_2 \tag{25}$$

$$h_{TP} = c_1 \left(Bo^2 We_f \frac{\rho_g}{\rho_f} \right)^{c_2} = c_1 K_2^{\,c_2} \tag{26}$$
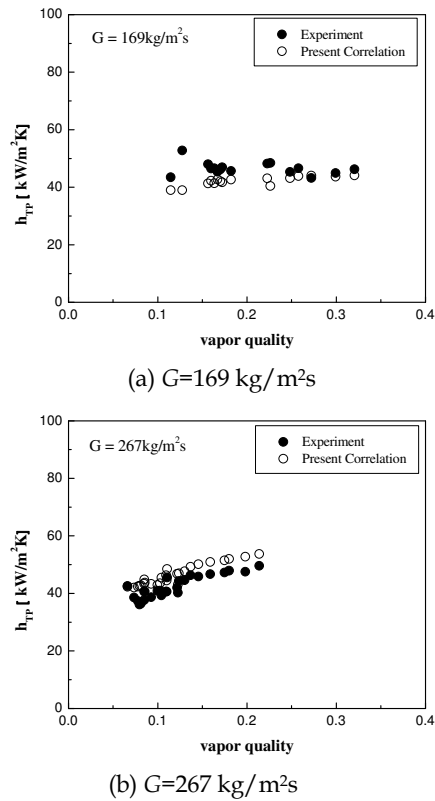
(a) G=169 kg/m²s

(b) G=267 kg/m²s

Fig. 13. Comparison of the experimental boiling heat transfer coefficients and the predictions of the new proposed correlation

The unknown constants c_1 and c_2 are determined from the experimental data. Finally, the following simple correlation having a unit of kW/m²K can be developed:

$$h_{TP} = 7.0 \times 10^3 \left(Bo^2 We_f \right)^{0.2} \left(\frac{\rho_g}{\rho_f} \right)^{0.2}$$

$$= 7.0 \times 10^3 \, K_2^{0.2} \tag{27}$$

To account for the weak dependency of the flow boiling heat transfer coefficient on the mass flux and vapor quality and to consider the strong effect of the evaporation momentum and surface tension forces, we developed a new modified correlation for the flow boiling heat transfer using the boiling number and liquid Webber number. Although the new modified correlation shows that the boiling heat transfer coefficient tends to increase slightly with vapor quality, the new suggested correlation predicts the experimental data more accurately, as shown in Fig. 13. To assess the prediction accuracy of the new correlation, we evaluated the MAE and get the lowest value, 10.4 %, as shown in Fig. 14.
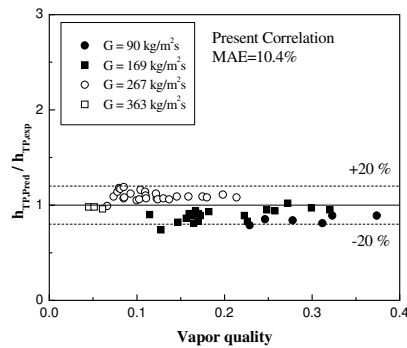
Fig. 14. Comparison of the flow boiling heat transfer coefficients with the predictions of the new correlation

3.4 Elongated bubble behavior

As shown in Figs. 9 and 10, an elongated bubble is important both from scientific and practical points of view in relation to microscale fluid flow and heat transfer problems. In other words, the elongated bubble behavior corresponds to heat transfer mechanism. The growth of the elongated bubble in the flow direction, both upstream and downstream, is governed by the major heat transfer mechanism in microchannel flow boiling (Huh et al., 2007).

Figure 15 shows sequential images of elongated bubble growth at a mass flux G=130 kg/m²s and a heat flux q''=195 kW/m². Different movements of the leading and trailing liquid-vapor interfaces were observed, indicating the elongated bubble grew not only in the flow direction but also counter to the bulk fluid flow direction.
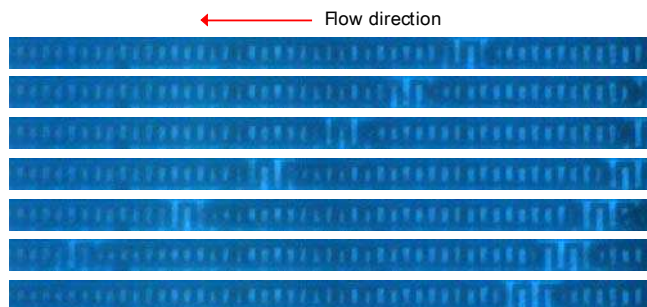

Fig. 15. Growth of an elongated bubble at G=130 kg/m²s and q''=195 kW/m² (time span between successive images =1.0 ·10⁻⁴ s) (Huh et al., 2007)

A numerical calculation of the elongated bubble growth was performed using Eqs. (28) and (29) of two-zone model (Jacobi and Thome, 2002), as shown in Fig. 16. The initial conditions which are the length of the elongated bubble/liquid slug pair were obtained from the experimental visualization results. The nucleation superheat, was obtained from the measured heated wall temperature. The two-zone model was originally developed for a circular microchannel under axially uniform heating conditions. However, the present rectangular microchannel was under nonuniform circumferential heating conditions. Since the PDMS has a thermal conductivity as low as 0.15 W/mK, the side and top wall of the

microchannel could be considered insulated. This modification to the heated area was considered in the numerical calculations. In circular uniformly heated microchannel, the heat transfer area was described as the internal surface area (i.e. product of circumference and length). On the other hand, the heat transfer area in single-side heated rectangular microchannel could be expressed as product of width and length of heated channel wall only when the non-heated wall could be treated as insulated state. Therefore, the coupled differential equations for the vapor and liquid can be modified:

$$\frac{dL_g}{dt} = \frac{q'' W_{ch} \left(L_g(t) + L_f(t) \right)}{\rho_g \pi \left(R - \delta_o \right)^2 i_{fg}} \tag{28}$$

$$\frac{dL_f}{dt} = -\frac{q'' W_{ch} \left(L_g(t) + L_f(t) \right)}{\rho_f \pi \left(R - \delta_o \right)^2 i_{fg}} \tag{29}$$
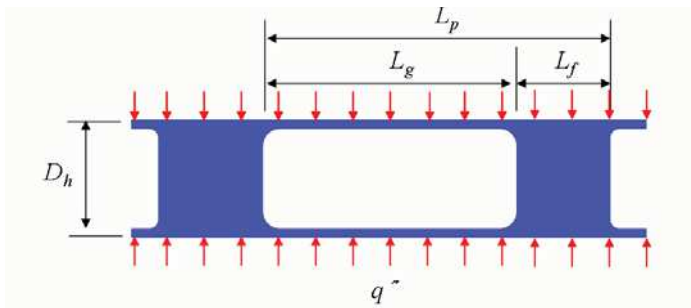

Fig. 16. The elongated bubble/liquid slug flow of two-zone model (Jacobi & Thome, 2002)

The elongated bubble lengths are compared to the experimental data in Fig. 17. The modified heating area calculations represented the experimental behavior well. Therefore, this modification was applied to the following calculations. The other variable parameter, the initial film thickness, was assumed to be one-tenth of the hydraulic diameter.
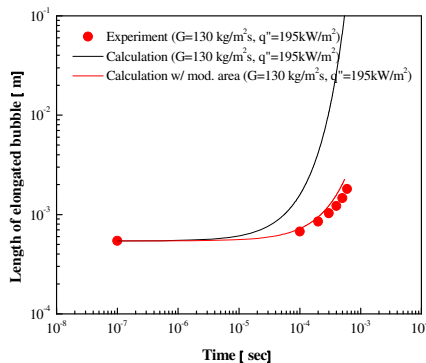

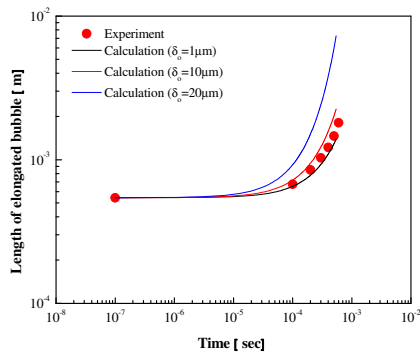Fig. 17. Length of an elongated bubble at G=130 kg/m²s and q''=195 kW/m² (Huh et al., 2007)

Fig. 18. Effect of the initial film thickness on the elongated bubble growth at G=130 kg/m²s and q''=195 kW/m² (Huh et al., 2007)

At present, the initial film thickness is difficult to measure directly. Figure 18 shows the effect of the initial liquid film thickness on the elongated bubble growth behavior. The initial film thicknesses between 1 µm and 10 µm showed similar behaviors; however, thicker initial film thicknesses produced unreasonable bubble growth estimations.

As the mass flux increased and the heat flux decreased, the calculated results gave a higher growth rate for the elongated bubble. This difference implies that the numerical two-zone model predicted fast elongated bubble growth behavior compared experiment. In other words, the two-zone model did not provide a reliable prediction capability as the vapor fraction decreased. On the other hand, the higher vapor fractions produced a thin liquid film flow along the heated wall and vapor flow in the core of microchannel, so that the thin liquid film evaporation in the two-zone model could predict the elongated bubble behavior (Huh et al., 2007).

4. Conclusion

In conclusion, experiments were performed to measure and predict two-phase pressure drop of flow boiling in a microchannel. Tests were performed over a mass flux of 90 to 363 kg/m²s and a heat flux of 200 to 700 kW/m². Test results were used to develop a new modified correlation to represent the two-phase frictional pressure drop and flow boiling heat transfer coefficient in a single horizontal rectangular microchannel. Finally, the elongated bubble growth behavior in a microchannel was analyzed by comparing experimental observations and numerical calculations under experimental initial conditions. The key findings from the study are as follows.

1. The two-phase frictional pressure drop increased with the heat flux and vapor quality. Most previous macro and mini/microchannel correlations did not provide reliable predictions except under certain limited conditions. A modified new two-phase frictional pressure gradient correlation using two-phase multiplier and the Martinelli parameter was proposed.
2. The measured flow boiling heat transfer coefficients slightly increased with vapor quality until x = 0.15 and were independent of the mass flux and vapor quality for high quality, 0.4 > x > 0.15. For lower vapor quality region, the main flow pattern is rapid, long elongated slug bubble flow acting like annular flow which is unique to the

microchannel flow. For higher vapor quality region, the major flow pattern is slug-annular or annular flow.

3. The unique characteristics of flow boiling in a microchannel are the nucleate boiling-like heat transfer coefficient behavior and convective boiling-like flow patterns observed, which occur because the very fast, long elongated slug flow acts like annular flow.

4. Most reported macro- and mini/microchannel correlations do not provide sufficient prediction accuracy, except under limited conditions, due to the limitations of the small geometry and different flow regimes. A new modified flow boiling heat transfer coefficient correlation is proposed using the boiling number, liquid Webber number, and liquid-vapor density ratio.

5. The growth behavior of the long elongated bubbles was governed by thin film evaporation. In elongated bubble flow regime, the two-zone model represents the bubble behavior well as the vapor fraction increased. However, the two-zone should be corrected by considering different film profiles inside the microchannel and circumferentially non-uniform thermal boundary conditions.

5. Acknowledgment

6. References

Blevins, R.D. (1984). *Applied Fluid Dynamics Handbook*, Van Nostrand Reinhold Company, ISBN 0-442-21296-8, New York

Chisholm, D. (1967). A Theoretical Basis for the Lockhart-Martinelli Correlation for Two-phase Flow. *International Journal of Heat and Mass Transfer*, Vol.10, No.12, (December 1967), pp. 1767–1778, ISSN 0017-9310

Chisholm, D. (1973). Pressure Gradients due to Friction during the Flow of Evaporation Two-phase Mixtures in Smooth Tubes and Channels. *International Journal of Heat and Mass Transfer*, Vol.16, No.2, (February 1973), pp. 347–358, ISSN 0017-9310

Collier, J.G. & Thome, J.R. (1994). *Convective Boiling and Condensation* (3rd Ed.), Oxford University Press, ISBN 0-19-856296-9, U.K

Holman, J.P. (2001). *Experimental Methods for Engineers* (7th Ed.), McGraw-Hill, ISBN 0-07-118165-2, New York

Huh, C., Choi, C.W. & Kim, M.H. (2007). Elongated Bubble Behavior during Flow Boiling in a Microchannel, *Proceedings of The Eighteenth International Symposium on Transport Phenomena*, Daejeon, Korea, August 27-30, 2007

Huh, C. & Kim, M.H. (2006). An Experimental Investigation of Flow Boiling in an Asymmetrically Heated Rectangular Microchannel, *Experimental Thermal and Fluid Science*, Vol.30, No.8, (August 2006), pp. 775–784, ISSN 0894-1777

Jacobi, A.M. & Thome, J.R. (2002). Heat Transfer Model for Evaporation of Elongated Bubble Flows in Microchannels. *Journal of Heat Transfer*, Vol.124, No.6, (December 2002), pp. 1131-1136, ISSN 0022-1481

Kandlikar, S.G. (1990). A General Correlation for Saturated Two-phase Flow Boiling Heat Transfer inside Horizontal and Vertical Tubes. *Journal of Heat Transfer*, Vol.112, No.1, (February 1990), pp. 219–228, ISSN 0022-1481

Kandlikar, S.G. (2001). A Theoretical Model to Predict Pool Boiling CHF Incorporating Effects of Contact Angle and Orientation. *Journal of Heat Transfer*, Vol.123, No.6, (December 2001), pp. 1071-1079, ISSN 0022-1481

Kandlikar, S.G. (2004). Heat Transfer Mechanisms during Flow Boiling in Microchannels. *Journal of Heat Transfer*, Vol.126, No.1, (February 2004), pp. 8-16, ISSN 0022-1481

Kandlikar, S.G., Shoji, M. & Dhir, V.K. (1999), Flow Boiling in Circular Tubes, In: *Handbook of Boiling and Condensation*, Taylor and Francis, ISBN 1-56032-634-4, NY

Kew, P.A. & Cornwell, K. (1997). Correlation for the Prediction of Boiling Heat Transfer in Small-diameter Channels. *Applied Thermal Engineering*, Vol.17, No.8-10, (August-October 1997), pp. 705-715, ISSN 1359-4311

Lazarek, G.M. & Black, S.H. (1982). Evaporative Heat Transfer, Pressure Drop and Critical Heat Flux in a Small Vertical Tube with R-113. *International Journal of Heat and Mass Transfer*, Vol.25, No.7, (July 1982), pp. 945–960, ISSN 0017-9310

Lee, H.J. & Lee, S.Y. (2001). Heat Transfer Correlation for Boiling Flows in Small Horizontal Channels with Low Aspect Ratios. *International Journal of Multiphase Flow*, Vol.27, No.12, (December 2001), pp. 2043-2062, ISSN 0301-9322

Lee, H.J. & Lee, S.Y. (2001). Pressure Drop Correlations for Two-phase Flow within Horizontal Channels with Small Heights. *International Journal of Multiphase Flow*, Vol.27, No.5, (May 2001), pp. 783-796, ISSN 0301-9322

Mishima, K. Hibiki, T. & Nishhara, H. (1993). Some Characteristics of Gas–liquid Flow in Narrow Rectangular Ducts. *International Journal of Multiphase Flow*, Vol.19, No.1, (February 1993), pp. 115–124, ISSN 0301-9322

Mishima, K. & Hibiki, T. (1996). Some Characteristics of Air–water Two-phase Flow in Small Diameter Vertical Tubes. *International Journal of Multiphase Flow*, Vol.22, No.4, (August 1996), pp. 703–712, ISSN 0301-9322

NIST Chemistry WebBook, Available from: <http://webbook.nist.gov/>

Qu, W. & Mudawar, I. (2003). Flow Boiling Heat Transfer in Two-phase Micro-channel Heat Sinks-I. Experimental Investigation and Assessment of Correlation Methods. *International Journal of Heat and Mass Transfer*, Vol.46, No.15, (July 2003), pp. 2755-2771, ISSN 0017-9310

Qu, W. & Mudawar, I. (2003). Measurement and Prediction of Pressure Drop in Two-phase Micro-channel Heat Sinks. *International Journal of Heat and Mass Transfer*, Vol.46, No.15, (July 2003), pp. 2737-2753, ISSN 0017-9310

Shah, R.K. & London, A.L. (1978). *Laminar Flow Forced Convection in Ducts: A Source Book for Compact Heat Exchanger Analytical Data*, Academic press, ISBN 978-0120200511, New York

Tran, T.N., Chyu, M.C., Wambsganss, M.W. & France, D.M. (2000). Two-phase Pressure Drop of Refrigerants during Flow Boiling in Small Channels: An Experimental Investigation and Correlation Development. *International Journal of Multiphase Flow*, Vol.26, No.11, (November 2000), pp. 1739–1754, ISSN 0301-9322

Tran, T.N., Wambsganss, M.W. & France, D.M. (1996). Small Circular- and Rectangular-Channel Boiling with Two Refrigerants. *International Journal of Multiphase Flow*, Vol.22, No.3, (June 1996), pp. 485-498, ISSN 0301-9322

Warrier, G.R., Dhir, V.K. & Momoda, L.A. (2002). Heat Transfer and Pressure Drop in Narrow Rectangular Channel. *Experimental Thermal and Fluid Science*, Vol.26, No.1, (April 2002), pp. 53–64, ISSN 0894-1777

Whalley, P.B. (1987). *Boiling, Condensation, and Gas-liquid Flow*, Clarendon Press, ISBN 0-19-856181-4, Oxford, UK

Yan, Y.Y. & Lin, T.F. (1998). Evaporation Heat Transfer and Pressure Drop of Refrigerant R-134a in a Small Pipe. *International Journal of Heat and Mass Transfer*, Vol.41, No.24, (October 1998), pp. 4183–4194, ISSN 0017-9310

Yu W., France, D.M., Wambsganss, M.W. & Hull, J.R. (2002). Twophase Pressure Drop, Boiling Heat Transfer, and Critical Heat Flux to Water in a Small-diameter Horizontal Tube. *International Journal of Multiphase Flow*, Vol.28, No.6, (June 2002), pp. 927–941, ISSN 0301-9322
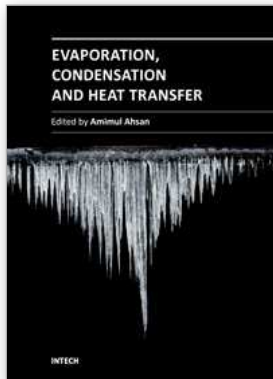
Evaporation, Condensation and Heat transfer

Edited by Dr. Amimul Ahsan

The theoretical analysis and modeling of heat and mass transfer rates produced in evaporation and condensation processes are significant issues in a design of wide range of industrial processes and devices. This book includes 25 advanced and revised contributions, and it covers mainly (1) evaporation and boiling, (2) condensation and cooling, (3) heat transfer and exchanger, and (4) fluid and flow. The readers of this book will appreciate the current issues of modeling on evaporation, water vapor condensation, heat transfer and exchanger, and on fluid flow in different aspects. The approaches would be applicable in various industrial purposes as well. The advanced idea and information described here will be fruitful for the readers to find a sustainable solution in an industrialized society.

How to reference

In order to correctly reference this scholarly work, feel free to copy and paste the following:

Cheol Huh and Moo Hwan Kim (2011). Flow Boiling in an Asymmetrically Heated Single Rectangular Microchannel, Evaporation, Condensation and Heat transfer, Dr. Amimul Ahsan (Ed.), ISBN: 978-953-307-583-9, InTech, Available from: http://www.intechopen.com/books/evaporation-condensation-and-heat-transfer/flow-boiling-in-an-asymmetrically-heated-single-rectangular-microchannel

INTECH
open science | open minds